NASA Technical Memorandum 100961

Contact Force History and Dynamic Response Due to the Impact of a Soft Projectile

J.E. Grady
Lewis Research Center
Cleveland, Ohio

August 1988

NASA

CONTACT FORCE HISTORY AND DYNAMIC RESPONSE DUE TO THE

IMPACT OF A SOFT PROJECTILE

J.E. Grady
National Aeronautics and Space Administration
Lewis Research Center
Cleveland, Ohio 44135

SUMMARY

A series of ballistic impact tests on several different instrumented targets was performed to characterize the dynamic contact force history resulting from the impact of a compliant projectile. The results show that the variation of contact force history with impact velocity does not follow the trends predicted by classical impact models. An empirical model was therefore developed to describe this behavior. This model was then used in a finite-element analysis to estimate the force history and calculate the resulting dynamic strain response in a transversely impacted composite laminate.

INTRODUCTION

As the use of composites becomes more common in modern aircraft, the performance of these materials under the full spectrum of loads they may encounter in advanced aerospace structural applications is of prime concern. Composite laminates are susceptible to impact damage, particularly that due to transverse impact. Bird strikes, for example, on aircraft flying at high speed and low altitude have recently proven to be extremely hazardous. Classical impact mechanics have been developed largely under the assumption of relatively stiff impactors which undergo small elastic deformations during the impact event. Energy dissipation and large deformations encountered during the high-speed impact of a more compliant projectile, such as a bird, limits the applicability of these classical approaches.

The objectives of this work are, first, to describe a simple experimental technique that can be used to determine the force history resulting from the impact of a soft projectile. Secondly, the data taken from a series of tests will be presented, interpreted, and used to form the basis of an empirical force-history model which will be used to analyze the transverse impact of a laminated beam.

In the first section of this report, a detailed description of the experimental apparatus and procedure is given. The next two sections outline an accurate and efficient numerical model that is used to analyze the impact experiment. The results of a simple "calibration test" are then compared with those from the numerical analysis to demonstrate the validity of the test procedure. In the following section, the measured response from the impact of the soft projectile is compared to the simpler classical model, and the fundamental differences between the two are established. An empirical model describing the contact force history due to the soft projectile impact is then devised and adapted to describe the more complicated transverse impact of the

composite laminate. A comparison of the dynamic strain response measured during an impact test of a composite specimen with that calculated by the finite element analysis is then used to assess the accuracy of the empirical force history model. Finally, a general discussion of the results is presented, followed by the conclusions.

EXPERIMENTAL APPARATUS AND PROCEDURE

Longitudinal stress waves propagate nondispersively in a uniform thin bar. An instrumented bar is therefore well suited to determining the force history due to longitudinal impact (refs. 1 and 2).

The experimental apparatus used here is shown in figure 1. The target is a uniform aluminum 6061-T6 bar of length 36 in., with a half-inch diameter circular cross section. Two electrical resistance foil-type strain gages (Micro-Measurements type EA-13-062AQ-350) are mounted in series at diametrically opposing points at the midpoint of the bar. This gage arrangement was chosen so as to eliminate the effect of any small flexural waves that would be generated by a slightly eccentric longitudinal impact. The bar is suspended using lightweight 24-gage wire at two support points located at 12 and 24 in. from either end. This allows the bar to swing freely in the longitudinal direction after the impact occurs, and results in a true free-free boundary condition for the bar. A 1-in. diameter aluminum end cap was installed on the proximal end of the bar, as shown in figure 2. The purpose of the end cap is to transfer the compressive force from the compliant impactor to the bar as the impactor deforms and flattens out to a greater diameter than that of the bar.

The impactors are fired at the bar from an air gun using compressed air, and the impact velocity is determined from the measured transit time between the two photoelectric diodes placed 10 in. apart halfway down the barrel of the air gun. Half-inch diameter silicon rubber balls with a nominal weight of 1.1 g are used as the impactors. They can be considered to be a generic representation of a "soft-body impactor." As the compressive strain pulse generated by the longitudinal impact passes the strain gages, the change in voltage output is amplified by the preamplifier, shown in figure 1; temporarily stored in the waveform recorder, and displayed on the oscilloscope. Permanent copies of the recorded signal are made on the plotter, and manually digitized records of the data are then stored on a computer for later analysis and plotting.

Numerical Analysis

A finite element program (ref. 3) was developed to perform a computational simulation of the longitudinal bar impact test. The results will lend additional physical insight into the problem and provide a basis of comparison for the experimental data. The bar was modeled with a series of four degree-of-freedom rod elements (ref. 4) which used the longitudinal displacements (u) and the corresponding strains (du/dx) at both nodal points as the degrees of freedom. The classical Hertz contact law was incorporated into the finite element program to define the force-displacement relation between the impactor and the bar. Newmark's implicit method of direct-time integration (refs. 5 and 6) was used to solve the equations of motion for the impactor and the bar simultaneously. The impactor was represented by a single degree of freedom lumped

mass connected to a uniaxial spring of stiffness given by Hertz's theory of elastic contact, which is summarized in the following section.

Hertz's Contact Law

Hertz derived the force-indentation relation to describe the elastic contact behavior between two spherical bodies. Hertz's contact law (refs. 7 and 8) is commonly used, in both static and dynamic applications, to determine the force arising from elastic contact. To briefly summarize Hertz's contact law, we have

$$F = K\alpha^n \tag{1}$$

where

F = contact force between spheres

α = relative indentation between spheres ($u_1 - u_2$)

n = 1.5

and

$$K = \frac{4}{3}\sqrt{\frac{R_1 R_2}{R_1 + R_2}} \left(\frac{k_1 k_2}{k_1 + k_2}\right) \tag{2}$$

where

R_i = radii of spheres

$$k_i = \frac{E_i}{1 - \nu_i^2}$$

and E_i, ν_i are the respective elastic constants. A schematic diagram of the assumed deformation during Hertzian contact is given in figure 3. A special case that is of interest here occurs when the target is flat ($R_2 = \infty$) in which case equation (2) simplifies to

$$K = \frac{4}{3}\sqrt{R_1}\left(\frac{k_1 k_2}{k_1 + k_2}\right) \tag{3}$$

Equation (3) is used in the finite element analysis as the effective spring constant in the simplified single-degree-of-freedom spring-mass representation of the impactor.

3

Calibration Test: Hertzian Impact

Before proceeding to the complicated problem of the high-speed impact of the soft projectile, a simpler case was considered. A preliminary test and corresponding analysis of the impact of a steel ball on the aluminum bar was performed to serve as a means of validating the experimental method. During a low-speed impact, the deformation should be mostly elastic, and thus the contact behavior between the steel and aluminum should be well described by the Hertz model.

Figure 4 shows the strain history measured at a single gage location on the bar during a 62.1 in./sec longitudinal impact. Comparison with the finite-element analysis using a 39-element (80 degrees of freedom) model of the bar and an integration time step of 0.5 μsec is very good. The contact force history is inferred from this strain measurement by multiplying the strain by the axial stiffness EA of the aluminum bar, and assuming that the initial pulse travels undistorted (nondispersively) through the bar. The impact force determined in this manner from the strain in figure 4 is compared with that calculated during the finite-element analysis in figure 5. Apparently, the finite-element model accurately calculates the strain history due to a Hertzian impact, and more importantly, the impact force can be determined directly from the measured strain. The effect on the impact force of varying the inertia of the target is also evident in figure 5. The increased mass of the end cap in the finite element model causes a corresponding increase in the maximum contact force, and a shift in the time at which the maximum force occurs. Figure 6 shows the subsequent propagation and reflection of the strain pulse along the bar, as calculated by the finite-element program. The free boundary condition causes the incident compressive pulse to reflect from the distal end of the bar as a tensile pulse of identical shape.

Longitudinal Impact With a Soft Projectile

In the previous section, a calibration test was used to verify that the contact force can be adequately estimated by simply multiplying the measured strain by the axial stiffness (EA) of the bar. The same bar is now used to measure the strain history resulting from the longitudinal impact of the half-inch diameter silicon rubber ball. The force history will then be calculated from the strain, and from here on will be referred to as the "measured force."

Figure 7 shows a typical measured impact force versus time behavior for the impact of the half-inch diameter silicon rubber ball. In contrast to the more nearly symmetrical Hertzian case, the shape of the curve is noticeably skewed. The force reaches its peak very early in the contact interval and then tapers off slowly before the impactor loses contact with the target. The Hertzian curve can be adequately characterized by a simple sine wave of amplitude F_O and duration T. The non-Hertzian behavior of the soft impactor, on the other hand, requires an additional parameter; t_{F_O}, the time at which the peak force occurs, to completely characterize its variation with time. Figure 7 identifies the three parameters on the measured curve.

A series of tests was performed to determine how the force history varied with impact velocity. Figures 8 to 10 show the variation in shape and amplitude of the force history resulting from impact of the half-inch ball on the

4

bar at velocities ranging from 1000 to 5000 in./s. Figure 8 shows that the amplitude of the force varies in proportion to V^2, which is in contrast to the nearly linear behavior predicted by the classical elastic impact models (ref. 9). Figure 9 shows that the contact time varies inversely with the impact velocity, also in contrast to the elastic models, which predict that the two are independent. In plotting this data, the effective "contact time," T, is taken as the duration of the large initial portion of the force history pulse, during which the majority of the impulse is transferred to the target. This approximation is shown in figure 7, and has the effect of ignoring the long trailing "tail" of the force history curve.

In figure 10, the relative "skewness," or shape, of the force history curve as indicated by the ratio t_{F_O}/T is shown to remain almost constant over the velocity range tested, although at very low velocities it approaches a more nearly symmetrical shape similar to the elastic case. This is reasonable, because at the lower velocities, the impactor will deform elastically for the most part and we would expect a correspondingly lower dissipation of energy to occur as a result of inelastic deformation of the impactor. Figure 11 shows that the impulse measured from the experimental data varies linearly with impact velocity, as would be expected. During a perfectly elastic impact with a rigid target, the projectile would rebound after impact with a velocity equal to its incident velocity, and the momentum transfer would be 2 mV. This line is shown for comparison in figure 11. Of course, a significant amount of energy dissipation occurs in this case as a result of damping in the impactor, rigid body motion (kinetic energy) of the bar, and the strain energy transferred to the bar during the collision, so the difference between the line I = 2 mV and the measured impulse only compares this experimental data with an ideal case, and in no way can be interpreted as a measure of experimental error.

A second series of tests was conducted with a 3/8-in. diameter impactor of the same material. The results are presented in figures 12 to 15 and indicate that the trends observed in the earlier series of tests do not depend on the impactor size, but instead are characteristic of the material, as we would expect. All measured data show the same trends as in the earlier series of tests. The numerical differences in the measured impact force histories are due to the smaller mass of the impactor. Having characterized the impact force resulting from the longitudinal impact of the rubber balls, a simple empirical model based on the data presented can be used to describe the force history and its variation with impact velocity. Assuming an approximate linear relationship for each of the curves shown in figures 8 to 15, we have

$$F_O = \alpha_1 \frac{mV^2}{2d} \tag{4}$$

$$T = \alpha_2 \frac{d}{V} \tag{5}$$

$$t_{F_O} = \alpha_3 T \tag{6}$$

$$I = \alpha_4 2mV \tag{7}$$

for both impactor sizes, where V, m, and d represent the impactor velocity, mass, and diameter, respectively; F_0, T, t_{F_0}, and I have their usual meanings; and the α_i are constants chosen to match the data. The values of α_i determined from figures 8 to 15 are given in table I.

TRANSVERSE IMPACT OF A LAMINATED BEAM

A simple empirical model has been developed to describe the contact force resulting from longitudinal impact of the soft projectile on a uniform bar. The problem of transverse impact on a composite laminate is of more practical interest, so this empirical model will now be extended to describe the latter case.

Experimental Apparatus and Procedure

Two composite laminates were tested. Both were composed of T300/934 graphite epoxy prepreg laid up in a symmetric cross-ply $[90/0]_{5s}$ configuration. The beam-like specimens were of different length but otherwise identical dimensions, and were supported in a cantilever fashion. They were instrumented with foil-type strain gages (type ED-DY-031CF-350, Sg = 3.25) at several locations, as shown in figure 16. Half-inch diameter silicon rubber balls were again used as the impactors for this series of tests. A high-speed FASTAX framing camera was used to photograph several tests. The camera has a maximum framing rate of 8000 frames per second. This rate was effectively doubled by using an internal rotating prism which made two exposures per frame, thus exposing 16 000 pictures per second. The impact firing sequence was initiated from a remotely operated test monitoring facility, with timers set to trigger the camera just prior to the impact event. A typical impact sequence as photographed from an edge-on view of the cantilevered specimen is shown in figure 17. The dynamic data measurement system shown in figure 1 was used to simultaneously record the transient strain signals at the two gage locations.

Finite-Element Model

The laminate was modeled with four-node isoparametric plain strain elements (ref. 10). Ideally, each lamina should be modeled with a number of finite elements to insure the best accuracy. However, such a procedure would lead to a formidably large number of elements for the 20-plied laminate. For this reason, the $[90/0]_{5s}$ laminate is transformed into an equivalent homogeneous plate with a set of effective moduli obtained by using the appropriate constant strain and constant stress assumptions (ref. 11). Six elements through the laminate thickness were found sufficient to accurately model the laminate bending stiffness. A typical segment of the uniform finite-element mesh is shown in figure 18. Each finite element represents several lamina. The effective elastic moduli of the elements was derived from the properties of the individual plies in reference 12. A convergence study was performed (ref. 3), and it was established that a uniform mesh of 1200 elements and 2800 total degrees of freedom, allowing two translational degrees of freedom at each nodal point, would provide a converged solution that accurately modeled the flexibility of the laminate.

It is evident from figure 17 that a large amount of deformation occurs in the rubber impactor while it is in contact with the laminate. This deformation spreads the load due to contact over a larger area than would occur with a more rigid impactor. In calculating the loading used in the finite-element model, this spatial distribution of the load must be accounted for if accurate predictions of the strain near the impact point are needed. This was accomplished in the following way.

For the purpose of modeling the variation of contact area with time, it is assumed that

$$A(t) = A_0 \frac{F(t)}{F_0} \tag{8}$$

where $A(t)$, $F(t)$ are the contact area and the contact force, respectively; and A_0, F_0 are their maximum values. This simplifying assumption is based on experimental measurements reported in reference 13 in which high-speed photography was used to measure the contact area of a similar rubber projectile as a function of time during a high-speed impact event. The shape of the area-versus-time curve is nearly identical to the force-history curve shown in figure 7. This evidence supports the implicit assumption made in equation (8) that the contact area varies in direct proportion to the contact force. The maximum contact area, A_0, can be measured experimentally from the circular imprint left on the laminate by the impactor. Because of the simplified two-dimensional finite-element representation of the target laminate, the impact load is taken to be uniformly distributed across the width of the laminate, as shown in figure 19, and the actual circular contact area of radius r must be approximated by a rectangular strip of dimension $2r \times 1$. Using equation (8) and

$$A(t) = \pi r^2(t) \tag{9}$$

we have

$$r(t) = r_0 \sqrt{\frac{F(t)}{F_0}} \tag{10}$$

where $r(t)$, r_0 are the contact radius and its maximum value. It is further assumed that the spatial force distribution $f(r)$ over the contact length at any given time is as shown in figure 20. Hence,

$$f(r,t) = F_{max}(t) \cdot \cos\left(\frac{\pi}{2}\frac{r}{r_0}\right), \quad r < r_0 \tag{11}$$

where F_{max} is the maximum force at any given time, and is assumed to occur at the center of contact. To calculate the discrete nodal force distribution for the finite-element analysis, we have, referring to figure 20,

$$f_i(t) = \int_{r_i - \Delta r/2}^{r_i + \Delta r/2} f(r,t)\, dr \tag{12}$$

7

where f_i represent the time dependent forces applied at the nodal points of the finite-element model. After imposing the condition

$$\int_{-r_o}^{+r_o} f(r,t) \, dr = F(t) \tag{13}$$

where F is the total force at the given time as referred to in equation (8), we can now reduce equation (12) to

$$f_i(t) = \frac{1}{2} F(t) \left[\sin \frac{\pi}{4r_o} (2r_i + \Delta r) - \sin \frac{\pi}{4r_o} (2r_i - \Delta r) \right] \tag{14}$$

The nodal force distribution is thus defined in terms of the total force transferred by the impact at a given time and the radial distance of the nodal point from the center of impact.

The temporal distribution of impact force must now be determined for the transverse impact case. The empirical relations given in equations (4) to (7) for the longitudinal impact case cannot be used directly because of the different stiffness of the target. However, it can be assumed that the impactor behaves in a similar manner in both cases. The skewed curve shown by the dashed line in figure 7 will therefore be assumed to qualitatively describe the force history during transverse impact. To calculate a curve of this general shape, the following force-versus-time relationship was incorporated into the finite-element computer program:

$$F(t) = \begin{cases} F_o \sin \left[\dfrac{\pi t}{2t_{F_o}} \right]; & 0 < t < t_{F_o} \\[2em] F_o \cos \left[\dfrac{\pi \left(t - t_{F_o} \right)}{2 \left(T - t_{F_o} \right)} \right]; & t_{F_o} < t < T \\[2em] 0 & ; \quad t > T \end{cases} \tag{15}$$

where F_o is the maximum force, t_{F_o} is the time when the maximum force occurs, and T is the contact duration.

Impact Force History

The empirical description of the impact force history measured from the bar tests and described by equation (15) is now adapted to predict the effective force history for the transverse impact of a composite beam. The following experimental/numerical method was used.

8

Strain histories were measured at the two gage locations on the composite laminate at a series of impact velocities from 1000 to 5000 in./sec. The finite-element model described previously was then used to model the impacted beam and calculate the strains at the two gage locations. The assumed force history in the finite-element analysis was varied, using the trends established in the earlier tests and shown in figures 8 to 10, in order to match the measured strain response. The following step-by-step procedure was followed:

(1) For a given impact velocity, input the force history measured from the longitudinal bar test into the finite-element program.

(2) Because the bar is slightly stiffer in the longitudinal direction than the laminate is in the transverse direction, the force in step 1 will be slightly overestimated. Decrease the peak force, F_o, by a factor corresponding to the difference between the calculated and measured strain amplitudes.

(3) The difference in stiffness of the targets also results in a slightly shorter contact time for the longitudinal impact. Keeping the ratio t_{F_o}/T constant, increase the contact duration, T, in the finite-element input by a factor corresponding to the difference between the measured and calculated first "zero crossing" for the bending strain (approximately 450 μs in fig. 21).

The resulting calculated bending strain closely approximates that measured experimentally. Comparisons at two gage locations for a 1166 in./s transverse impact are shown in figures 21 and 22. The clamped boundary in the experimental mounting fixture for the cantilevered specimen cannot realistically act as a perfectly rigid constraint. As a result, some of the kinetic energy of the specimen is dissipated through the boundary, and the contribution of reflected flexural wave motion from this boundary is overestimated by the finite-element model, which assumes a perfectly rigid condition. The appearance of reflected waves at the gage locations is apparent at approximately 200, 600, and 800 μs at gage 1 in figure 21, and at approximately 400 and 800 μs at gage 2 in figure 22.

After the steps outlined above have been followed, the modified force history will have a slightly lower maximum value and a slightly longer contact duration than was measured for the longitudinal bar tests. The variation of the resulting effective impact force histories with impact velocity is shown graphically in figures 23 to 25. Figures 23 and 24 indicate that the contact force is lower and the total contact time is longer in the shorter specimen, for a given impact velocity. This indicates that the flexural wave reflections from the boundaries have a significant effect on the force history. If the effect of the wave motion was not considered, and a single degree of freedom spring-mass model based on the static stiffness of the respective laminates was used to anticipate these trends in the force history, the opposite behavior would be predicted. Indeed, the shape of the force history also depends on the length of the target, as shown in figure 25. Comparing these results with those obtained from the longitudinal bar experiment shown in figures 8 to 15, it is apparent that the relationships between the impact velocity and the three parameters describing the force history are similar. That is, the maximum force varies in proportion to V^2, the contact duration varies inversely with V, and the ratio t_{F_o}/T is relatively constant over the velocity range tested.

The parameters describing the force histories indicated by the data points in figures 23 to 25 are tabulated in tables II and III.

CONCLUSIONS

A simple experiment to measure the force history resulting from the ballistic impact of a compliant projectile was described. The results show that for the compliant rubber impactor used here, the velocity dependence of the force history is significantly different from that which would be predicted using classical impact mechanics. This is due primarily to the large deformation of the impactor, and the inelastic nature of the impact process.

Classical elastic impact mechanics predict a symmetrical variation of contact force with time, with a sine-wave type shape. In contrast, the shape of the curve describing the force due to impact of a more compliant projectile is noticeably skewed. The force reaches its peak very early in the contact interval and tapers off slowly before the impactor loses contact with the target. In contrast to the nearly linear behavior predicted by the elastic impact models, the force amplitude for the compliant projectile varies directly with the square of the impact velocity. In addition, the contact time was observed to decrease linearly with increasing impact velocity over the velocity range tested, whereas elastic models predict that contact time is independent of velocity.

An empirical model based on the experimental data was used to describe the contact behavior. This model was incorporated into a finite-element program to estimate the force history and resulting dynamic strain response at several locations on a transversely impacted composite laminate. The empirical representation of the data was shown by this means to accurately duplicate the actual impact force history. It was shown that the behavior of the impactor during the transverse impact of a laminated beam is similar qualitatively to that measured during the longitudinal impact of a bar of uniform circular cross section.

REFERENCES

1. Graff, K.F.: Wave Motion in Elastic Solids. Ohio State University Press, 1975, pp. 100-108, 133.

2. Baker, W.E.; and Dove, R.C.: Measurement of Internal Strains in a Bar Subjected to Longitudinal Impact. Exper. Mech., vol. 2, no. 10, Oct. 1962, pp. 307-311.

3. Grady, J.E.: Dynamic Delamination Crack Propagation in a Graphite/Epoxy Laminate. Ph.D. Thesis, Purdue University, 1985.

4. Yang, T.Y.; and Sun, C.T.: Finite Elements for the Vibration of Framed Shear Walls. J. Sound Vibr., vol. 27, no. 3, Apr. 8, 1973, pp. 297-311.

5. Newmark, N.M.: A Method of Computation for Structural Dynamics. ASCE J. Eng. Mech. Div., vol. 85, No. EM3, July 1959, pp. 67-94.

6. Cook, R.D.: Concepts and Applications of Finite Element Analysis. 2nd ed., John Wiley and Sons, 1981, pp. 320-325.

7. Hertz, H.: J. Mathematics, vol. 92, 1881.

8. Timoshenko, S.P.; and Goodier, J.N.: Theory of Elasticity. 3rd ed., McGraw-Hill, 1970.

9. Goldsmith, W.: Impact: The Theory and Physical Behavior of Colliding Solids. Edward Arnold Publishing, London, 1960.

10. Bathe, K.J.; Wilson, E.L.; and Peterson, F.E.: SAP-IV: A Structural Analysis Program for Static and Dynamic Response of Linear Systems. NSF EERC 73-11, California University, Berkeley, CA, Earthquake Engineering Research Center, June, 1973.

11. Jones, R.M.: Mechanics of Composite Materials. Scripta Book Co., Washington, D.C., 1975.

12. Sun, C.T.; and Grady, J.E.: Dynamic Delamination Fracture Toughness of a Graphite Epoxy Laminate Under Impact. Compos. Sci. Technol., vol. 31, no. 1, 1988, pp. 55-72.

13. Daniel, I.M.; Liber, T.; and LaBedz, R.H.: Wave Propagation in Transversely Impacted Composite Laminates. Exper. Mech., vol. 19, no. 1, Jan. 1979, pp. 9-16.

TABLE I. - EMPIRICAL CONSTANTS THAT DESCRIBE THE
MEASURED IMPACT FORCE HISTORY FOR LONGITUDINAL
IMPACT OF SILICON RUBBER PROJECTILES

Impactor diameter, d, in.	Scale parameters from longitudinal impact			
	$\alpha_1 = F_0 \frac{2d}{mV^2}$	$\alpha_2 = T \frac{V}{d}$	$\alpha_3 = \frac{t_{F_0}}{T}$	$\alpha_4 = \frac{I}{2mV}$
3/8	4.00	1.03	0.25	0.74
1/2	4.25	.93	.23	.66

TABLE II. - FORCE HISTORIES USED IN ANALYSIS
OF IMPACT ON LONG COMPOSITE BEAM SPECIMEN

Force history	V, in./s	F_0, lb	t_{F_0}, μs	T, μs	r_0, in.
1	1166	44	30	355	0.25
2	1932	90	21	250	.25
3	3058	215	13	158	.30
4	4026	325	10	120	.35

TABLE III. - FORCE HISTORIES USED IN ANALYSIS
OF IMPACT ON SHORT COMPOSITE BEAM SPECIMEN

Force history	V, in./s	F_0, lb	t_{F_0}, μs	T, μs	r_0, in.
1	1166	42	35	415	0.25
2	1981	84	20	310	.25
3	2994	170	13	205	.30
4	4049	245	10	155	.35
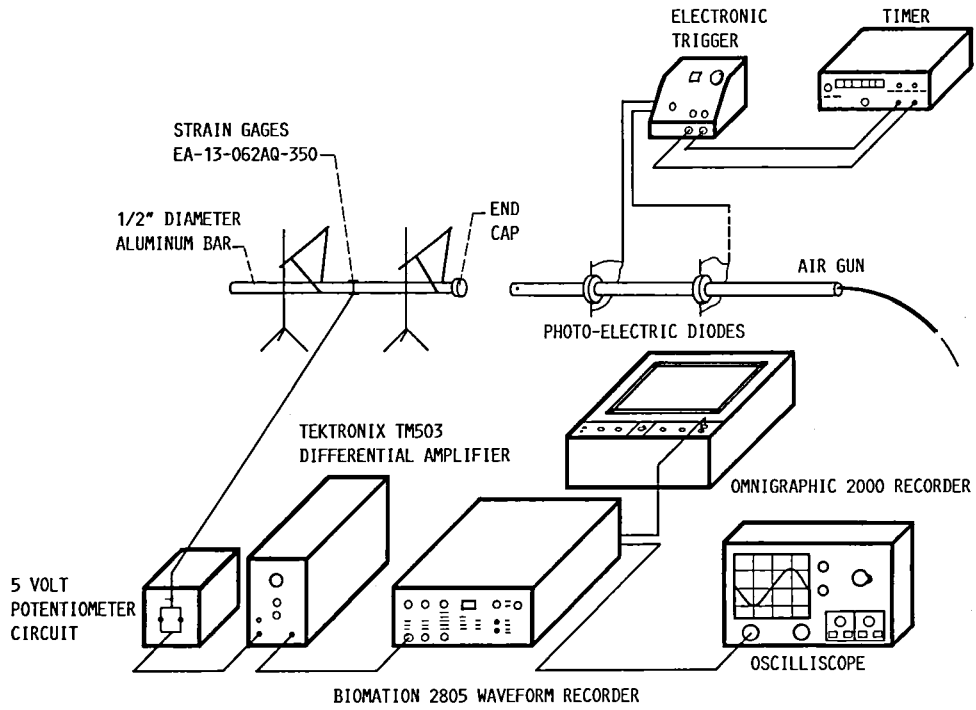
FIGURE 1. - LONGITUDINAL BAR EXPERIMENTAL SETUP.
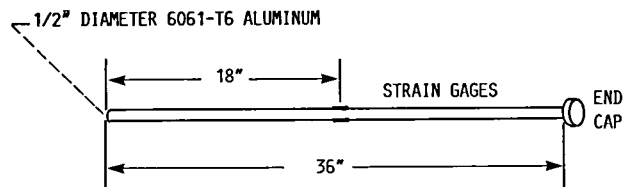
(A) BAR DETAIL.
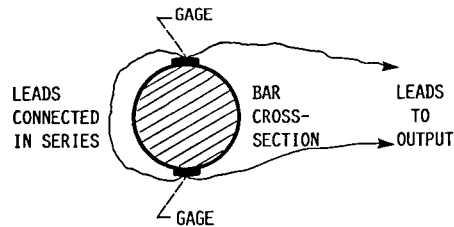
(B) STRAIN GAGE LOCATION AND SERIES WIRING.
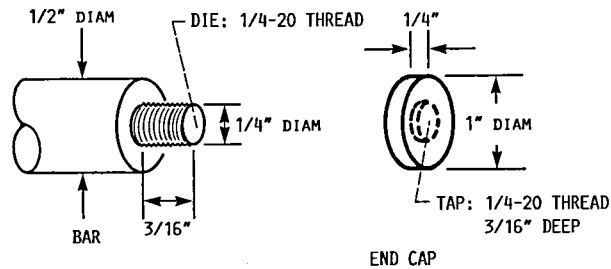
(C) END CAP FIXTURE DETAIL.

FIGURE 2. - BAR INSTRUMENTATION AND FIXTURING.
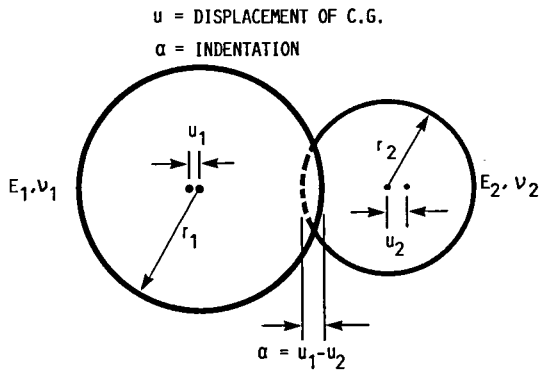
FIGURE 3. - HERTZIAN CONTACT BETWEEN TWO ELASTIC SPHERES.

u = DISPLACEMENT OF C.G.
α = INDENTATION

$\alpha = u_1 - u_2$
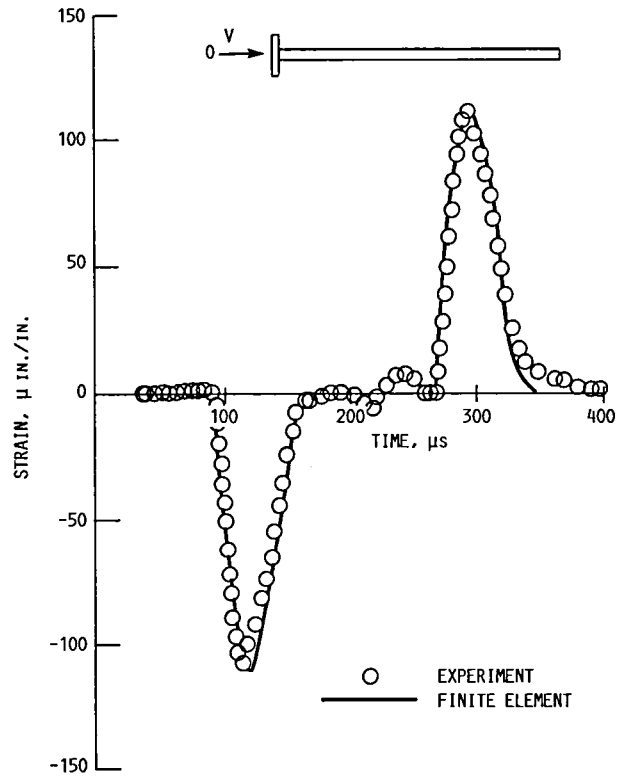
FIGURE 4. - STRAIN HISTORY AT MIDPOINT OF BAR FROM
62.1 IN./S IMPACT OF 5/8 IN. DIAMETER STEEL BALL.

○ EXPERIMENT
— FINITE ELEMENT

WITH END CAP
WITHOUT END CAP

○ EXPERIMENT
— FINITE ELEMENT
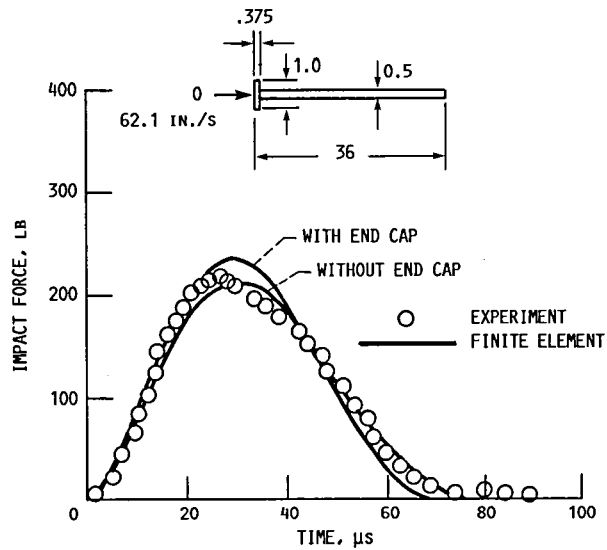
FIGURE 5. - FORCE HISTORY FROM 62.1 IN./S IMPACT OF
5/8 IN. DIAMETER STEEL BALL ON ALUMINUM BAR.

13
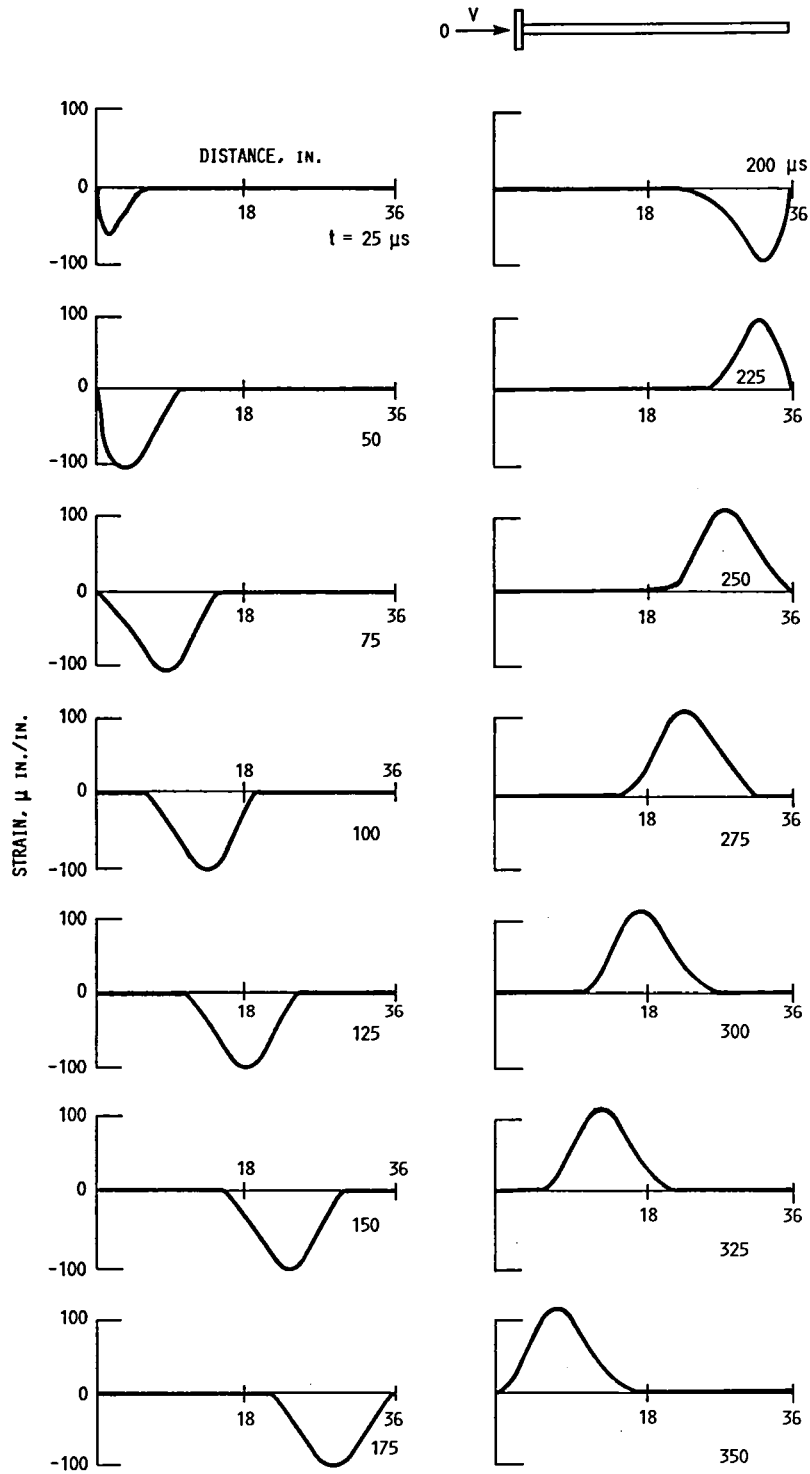
FIGURE 6. - PROPAGATION AND REFLECTION OF LONGITUDINAL STRAIN PULSE FROM
62.1 IN./S IMPACT OF 5/8 IN. DIAMETER STEEL BALL.
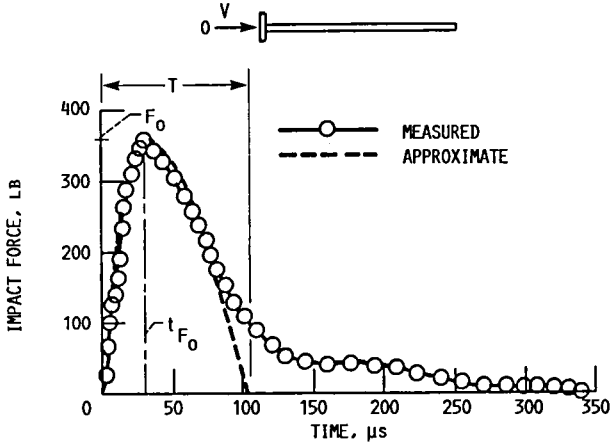
FIGURE 7. - FORCE HISTORY MEASURED FROM 3500 IN./s
IMPACT OF HALF-INCH DIAMETER SILICON RUBBER IMPACTOR.
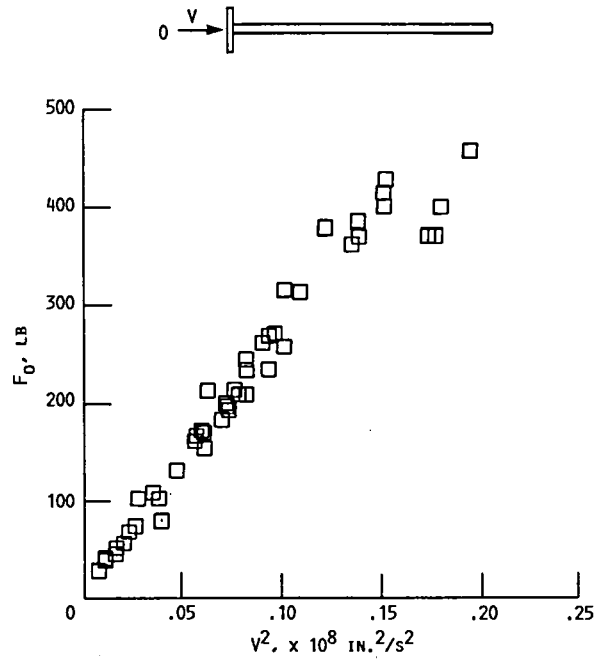
FIGURE 8. - MAXIMUM FORCE AMPLITUDE VERSUS V^2 FOR HALF-
INCH DIAMETER RUBBER IMPACTOR.
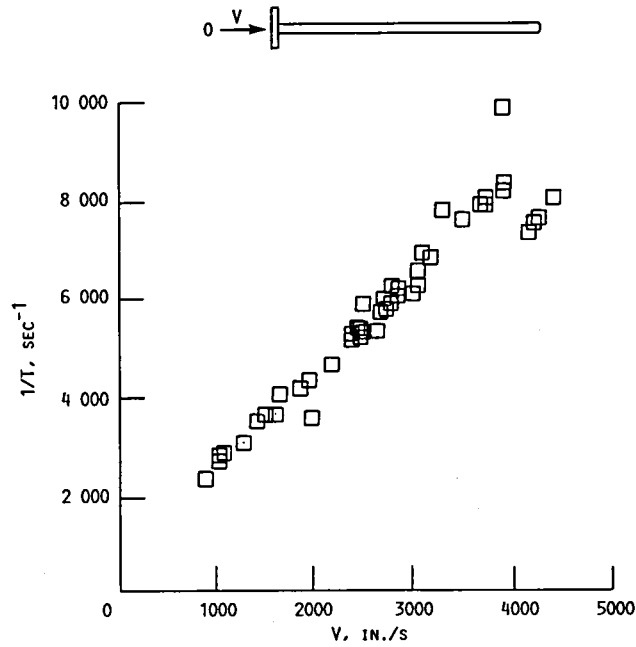
FIGURE 9. - INVERSE CONTACT TIME VERSUS IMPACT VE-
LOCITY FOR HALF-INCH RUBBER DIAMETER IMPACTOR.

15
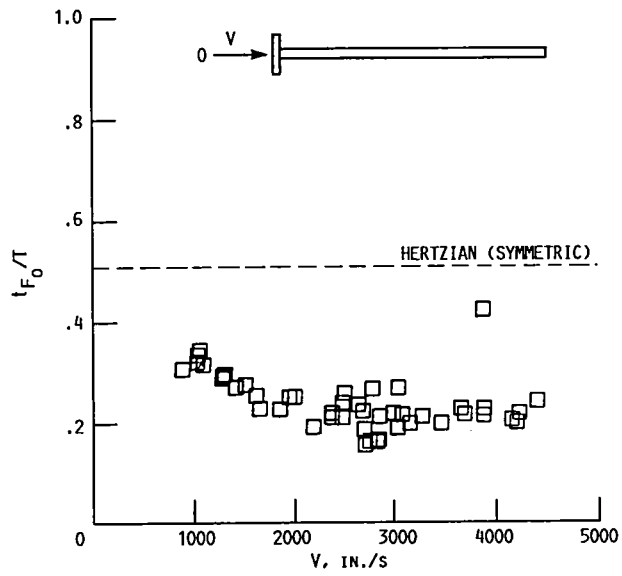
FIGURE 10. - t_{F_0}/T VERSUS IMPACT VELOCITY FOR HALF-
INCH DIAMETER RUBBER IMPACTOR.
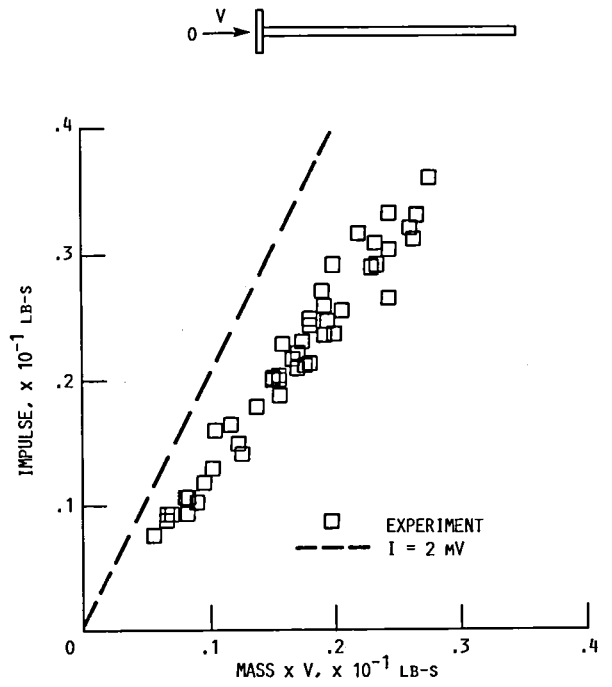
FIGURE 11. - MEASURED IMPULSE VERSUS INCIDENT MOMENTUM
FOR HALF-INCH DIAMETER RUBBER IMPACTOR.
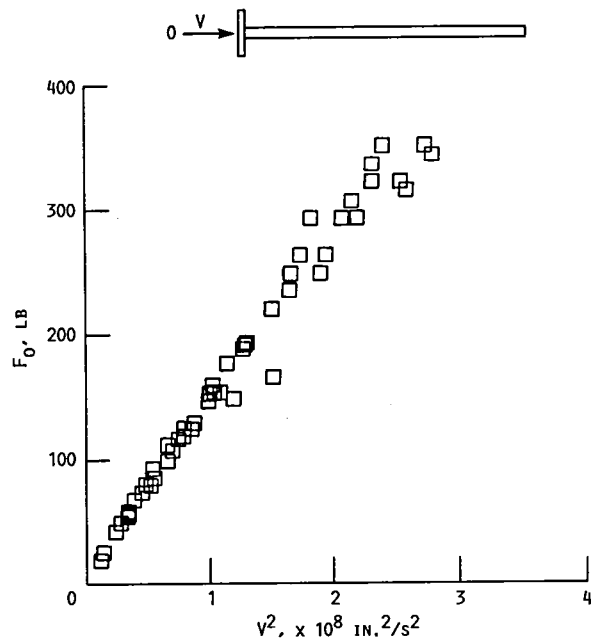
FIGURE 12. - MAXIMUM FORCE AMPLITUDE VERSUS V^2 FOR
3/8 IN. DIAMETER RUBBER IMPACTOR.

16
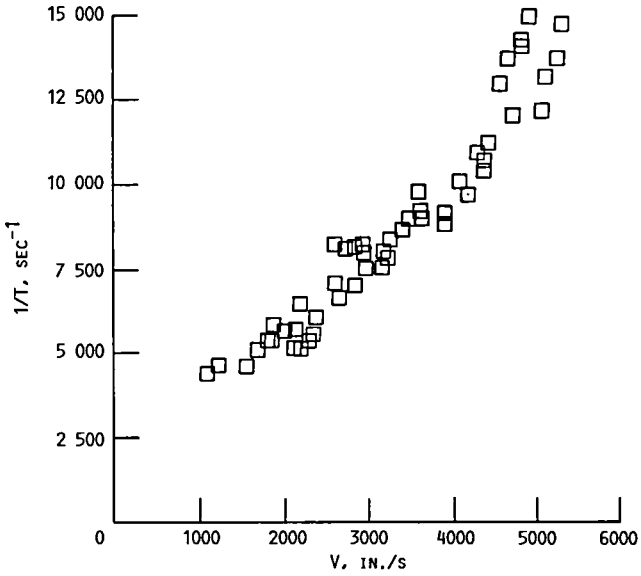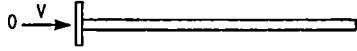
FIGURE 13. – INVERSE CONTACT TIME VERSUS IMPACT VE-
LOCITY FOR 3/8 IN. DIAMETER RUBBER IMPACTOR.
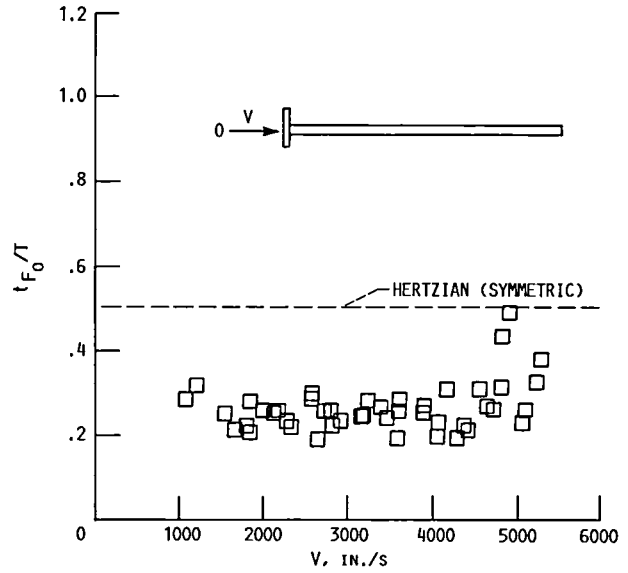
FIGURE 14. – t_{F_0}/T VERSUS IMPACT VELOCITY FOR 3/8 IN.
DIAMETER RUBBER IMPACTOR.
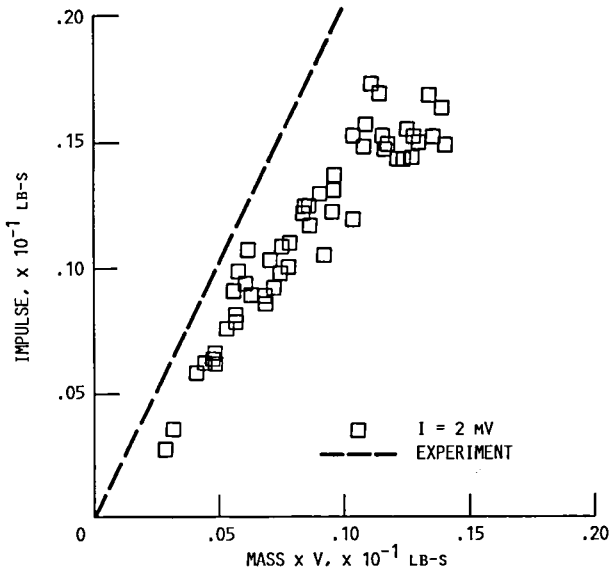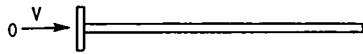
FIGURE 15. – MEASURED IMPULSE VERSUS INCIDENT MOMENTUM
FOR 3/8 IN. DIAMETER RUBBER IMPACTOR.
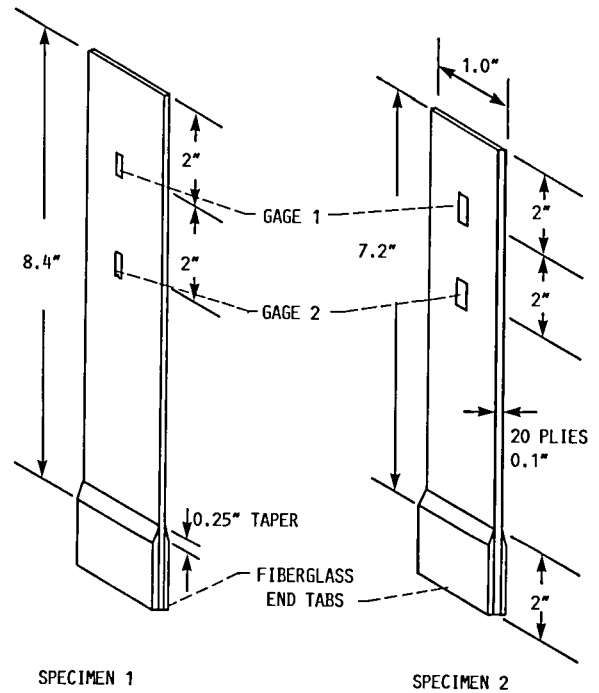
FIGURE 16. – STRAIN GAGE LOCATIONS ON CANTILEVER IMPACT
SPECIMENS.

17

0

FILMED REGION
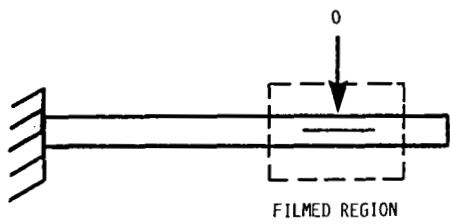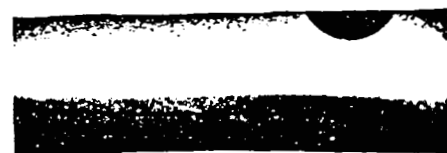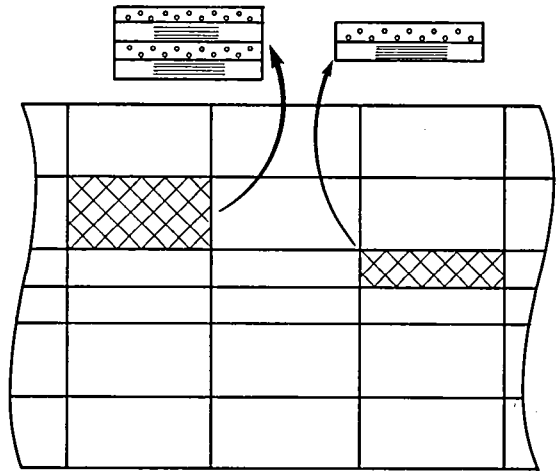
t = 62.5 µs
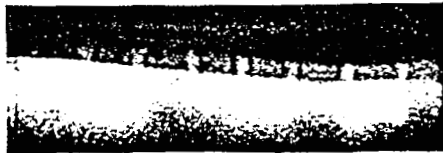
125
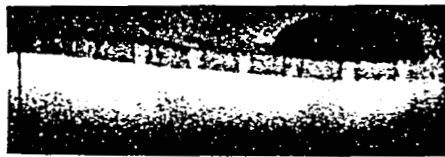
187.5

250

312.5
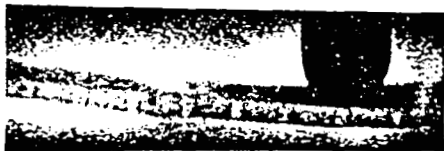
375

437.5

500

562.5
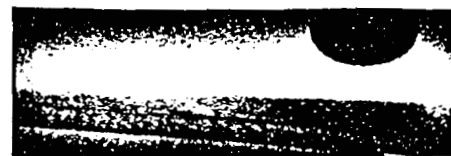
625

687.5
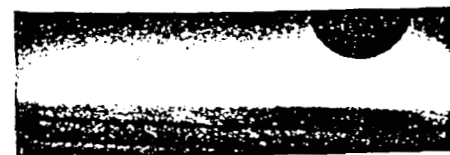
750

812.5

FIGURE 17. - TRANSVERSE IMPACT OF CANTILEVERED [90/0]$_{5S}$ COMPOSITE LAMINATE WITH 1/2" DIAMETER RUBBER BALL AT 6220 IN./S.

18

LAMINA PROPERTIES:

$E_1 = 19.5 \times 10^6$ PSI

$E_2 = 1.5 \times 10^6$ PSI

$G_{12} = 0.725 \times 10^6$ PSI

$\nu_{12} = \nu_{13} = \nu_{23} = 0.33$

$\rho = 1.49 \times 10^{-4}$ LB.s^2/IN.^{4}

FINITE ELEMENT CONSTANTS:

$\bar{E}_1 = \bar{E}_2 = 10.5 \times 10^6$ PSI

$\bar{E}_3 = 1.5 \times 10^6$ PSI

$\bar{G}_{12} = 0.725 \times 10^6$ PSI

$\bar{\nu}_{13} = \bar{\nu}_{23} = 0.33$

$\bar{\nu}_{12} = 0.05$

FIGURE 18. - FINITE ELEMENT DISCRETIZATION OF $[90/0]_{5s}$ GRAPHITE/EPOXY LAMINATE.

(A) ACTUAL CIRCULAR LOAD DISTRIBUTION.

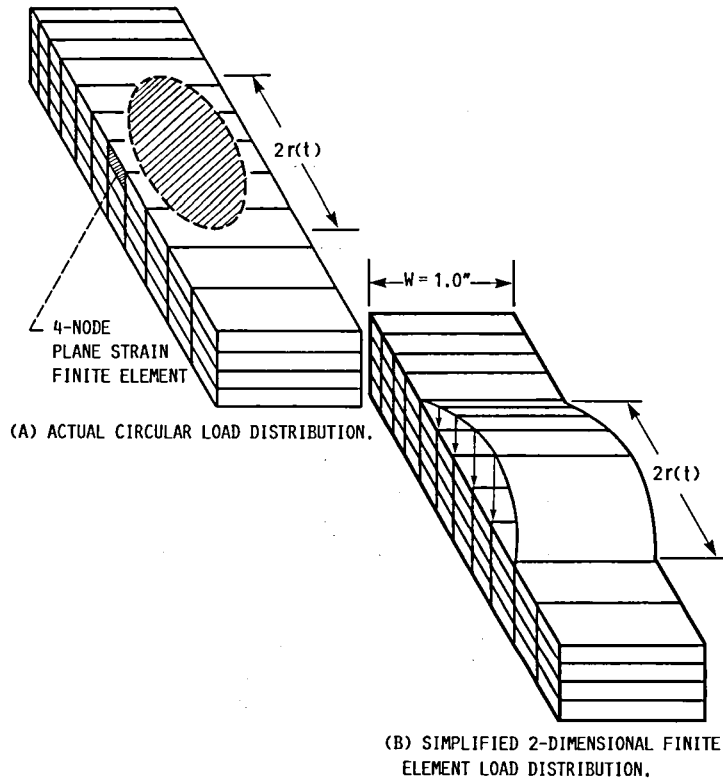(B) SIMPLIFIED 2-DIMENSIONAL FINITE ELEMENT LOAD DISTRIBUTION.

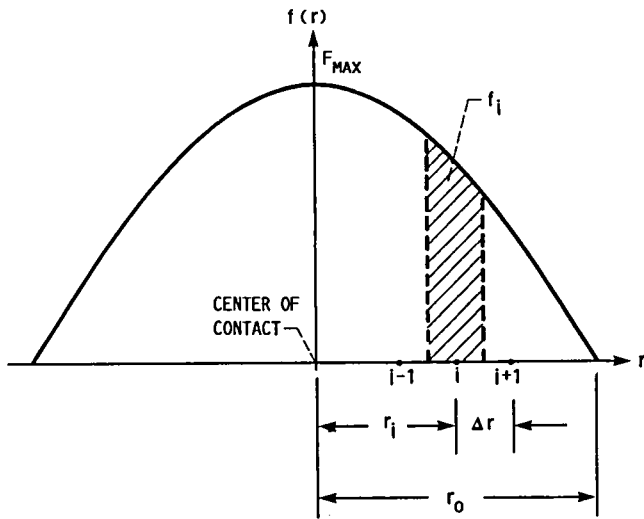FIGURE 19. - IMPACT LOAD DISTRIBUTION.

19

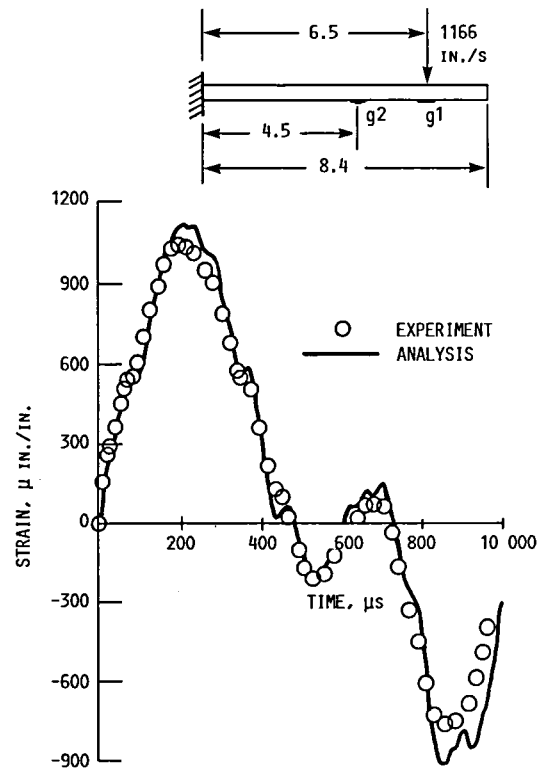FIGURE 20. - NODAL FORCE DISTRIBUTION AT FIXED INSTANT IN TIME.

FIGURE 21. - STRAIN HISTORY AT GAGE 1 IN LONG BEAM SPECIMEN USING FORCE HISTORY NUMBER 1.
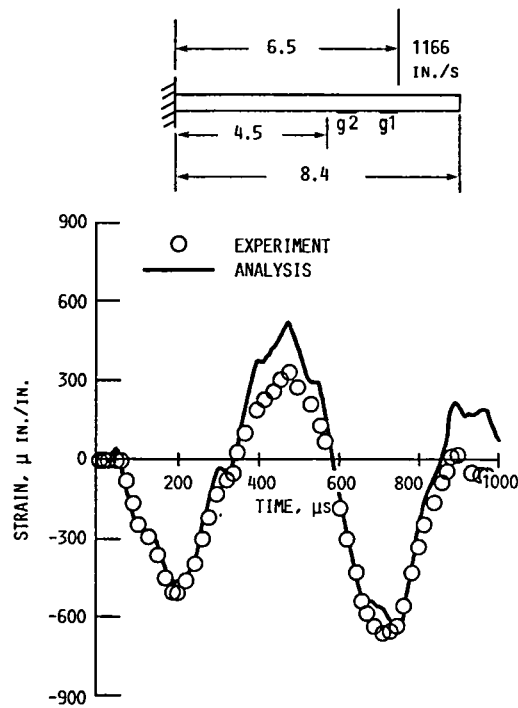

FIGURE 22. - STRAIN HISTORY AT GAGE 2 IN LONG BEAM SPECIMEN USING FORCE HISTORY NUMBER 1.
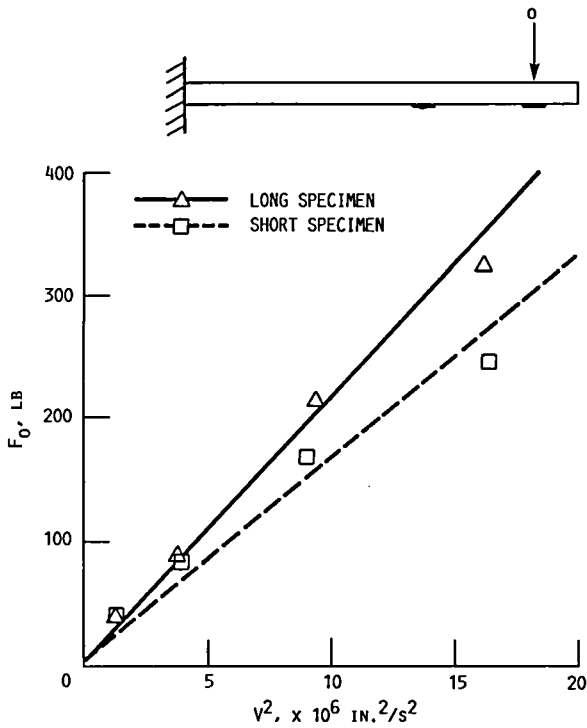
20

FIGURE 23. - FORCE AMPLITUDE VERSUS V^2 FOR IMPACT OF
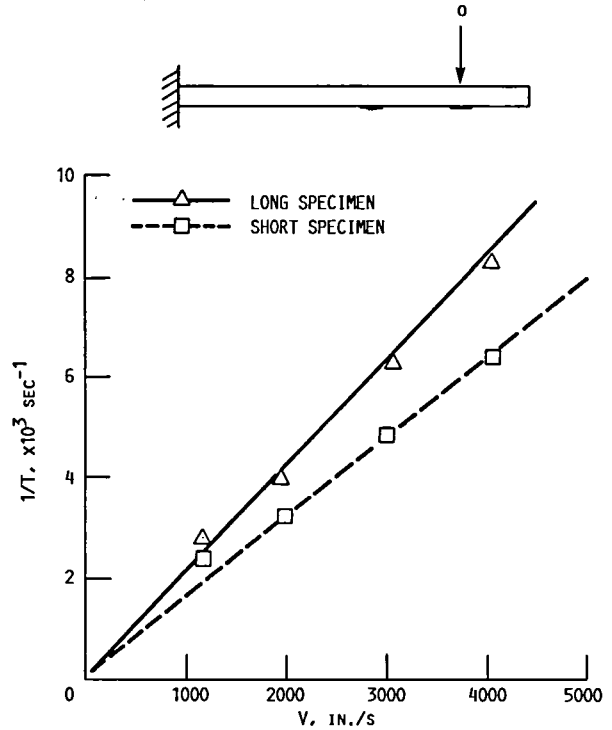1/2 IN. DIAMETER SILICON RUBBER BALL ON COMPOSITE
LAMINATES.

FIGURE 24. - INVERSE CONTACT TIME VERSUS IMPACT VE-
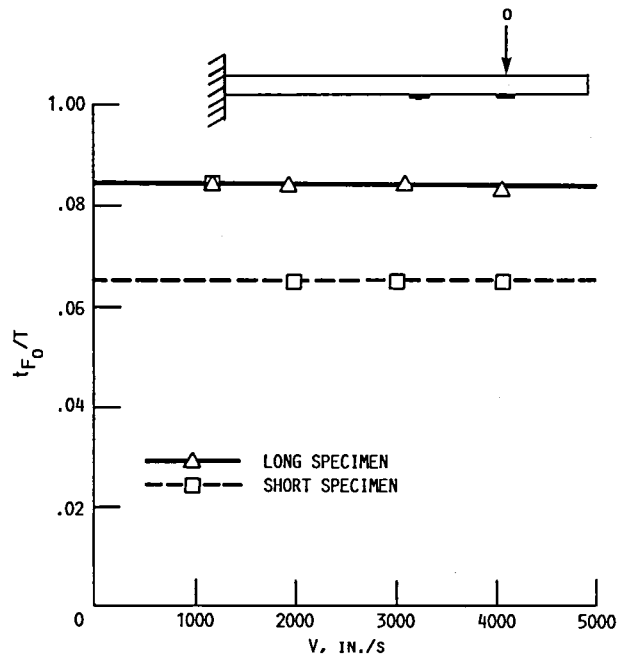LOCITY FOR IMPACT OF 1/2 IN. DIAMETER SILICON RUBBER
BALL ON COMPOSITE LAMINATES.

FIGURE 25. - t_{F_0}/T VERSUS IMPACT VELOCITY FOR IMPACT
OF 1/2 IN DIAMETER SILICON RUBBER BALL ON COMPOSITE
LAMINATES.

21

Report Documentation Page

1. Report No. NASA TM-100961	2. Government Accession No.	3. Recipient's Catalog No.
4. Title and Subtitle Contact Force History and Dynamic Response Due to the Impact of a Soft Projectile		5. Report Date August 1988
		6. Performing Organization Code
7. Author(s) J.E. Grady		8. Performing Organization Report No. E-4035
		10. Work Unit No. 505-63-11
9. Performing Organization Name and Address National Aeronautics and Space Administration Lewis Research Center Cleveland, Ohio 44135-3191		11. Contract or Grant No.
		13. Type of Report and Period Covered Technical Memorandum
12. Sponsoring Agency Name and Address National Aeronautics and Space Administration Washington, D.C. 20546-0001		
		14. Sponsoring Agency Code

15. Supplementary Notes

16. Abstract

A series of ballistic impact tests on several different instrumented targets was performed to characterize the dynamic contact force history resulting from the impact of a compliant projectile. The results show that the variation of contact force history with impact velocity does not follow the trends predicted by classical impact models. An empirical model was therefore developed to describe this behavior. This model was then used in a finite-element analysis to estimate the force history and calculate the resulting dynamic strain response in a transversely impacted composite laminate.

17. Key Words (Suggested by Author(s)) Impact; Wave propagation; Structural dynamics; Finite elements; Composite materials	18. Distribution Statement Unclassified - Unlimited Subject Category	
19. Security Classif. (of this report) Unclassified	20. Security Classif. (of this page) Unclassified	21. No of pages 22	22. Price* A02

National Aeronautics and
Space Administration

Lewis Research Center
Cleveland, Ohio 44135

Official Business
Penalty for Private Use $300

ADDRESS CORRECTION REQUESTED

U.S.MAIL

Postage and Fees Paid
National Aeronautics and
Space Administration
NASA 451

NASA

LIBRARY MATERIAL SLIP		
DO NOT REMOVE SLIP FROM MATERIAL		
Delete your name from this slip when returning material to the library.		
NAME	**DATE**	**MS**
S. Scotti	5/03	396
Library		185

NASA Langley Form 474 (Rev. Oct. 1999)